

# Bimodal Inhibition of Caspase-1 by Aryloxymethyl and Acyloxymethyl Ketones

Kenneth D. Brady\*

BASF Bioresearch Corporation, 100 Research Drive, Worcester, Massachusetts 01605-4314

Received February 10, 1998; Revised Manuscript Received April 13, 1998

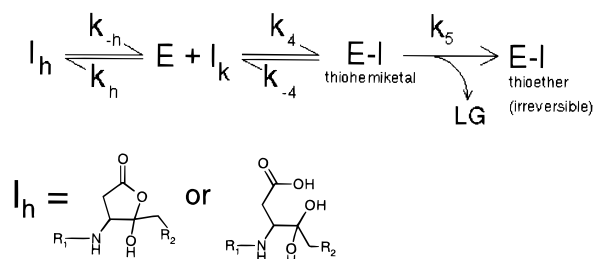
**ABSTRACT:** The caspase-1 (interleukin  $1\beta$ -converting enzyme; ICE) titrant 3-[2-(2-benzyloxycarbonylamino-3-methylbutyrylamino)propionylamino]-4-oxo-5-(2-oxo-2H-chromen-7-yloxy)pentanoic acid (**1** (Dang, L. C., et al. (1996) *Biochemistry* 35, 14910–14916)) inhibits caspase-1 activity rapidly, while release of the 7-hydroxycoumarin fluorophore is much slower. Progress curve analysis of **1** and of the related acyloxymethyl ketone 3-[2-(2-benzyloxycarbonylamino-3-methylbutyrylamino)propionylamino]-4-oxo-5-(1-oxo-3-phenylpropoxy)pentanoic acid (**2**) identifies distinctive residual patterns which are caused by the superimposition of potent slow-binding reversible inhibition with slower, irreversible inactivation. Standard kinetic models are not entirely adequate for analysis of these bimodal inhibitors, but by measuring the kinetic properties of these inhibitors by several independent techniques and comparing these to simulations which closely mimic the inhibitor actions, careful application of the standard models can provide reasonably accurate kinetic constants.

Cysteine proteases serve critical roles in diverse pathological processes and therefore represent attractive targets for pharmaceutical intervention (2, 3). The cysteine protease caspase-1 is essential for proper processing of the inflammatory cytokine interleukin- $1\beta$  and of interferon- $\gamma$ -inducing factor (4–6), and is likely to play important roles in septic shock (7, 8) and leukemias (9, 10).

An important advance in the field of cysteine protease inhibition was made with the discovery that certain weak electrophiles remain essentially nonreactive until oriented in the active site of target cysteine proteases (11–13). These “quiescent nucleofuge” inhibitors were then capable of reaction rates in excess of  $10^6 \text{ M}^{-1} \text{ s}^{-1}$ . Dolle and co-workers have since applied this strategy to the inhibition of caspase-1 and developed alternative leaving groups including phosphinic acids, 5-hydroxypyrazols, and tetronic acid derivatives (14–17). Aryloxymethyl ketones have also been described as potent inhibitors of caspase-1 (18, 19).

Many of the acyloxymethyl- and aryloxymethyl ketone inhibitors are time-dependent inhibitors of cysteine proteases. In some cases, second-order plots of  $k_{\text{obs}}$  vs [I] demonstrate saturation of the observed rate of inactivation (12, 19, 20), supporting the model shown in Scheme 1. We have reported the synthesis and use of an active-site titrant (**1**, Table 1) for caspase-1 which utilizes a fluorogenic hydroxycoumarin as the quiescent nucleofuge (I). This inhibitor permits observation in continuous assays both of the inhibitory effects on enzyme activity and of the release of 7-hydroxycoumarin, which corresponds to the irreversible step of Scheme 1. This report examines the actions of this titrant plus a small set of related compounds to demonstrate that these “bimodal”

Scheme 1



inhibitors display two distinct modes of inhibition. Analysis of the kinetic profiles of these inhibitors can be further complicated by slow onset of the reversible mode, but simulation studies demonstrate that the common kinetic models, cautiously applied, do provide reasonably accurate kinetic constants.

## MATERIALS AND METHODS

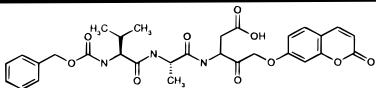
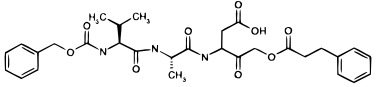
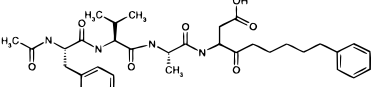
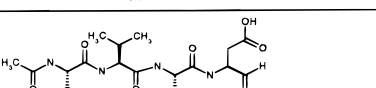
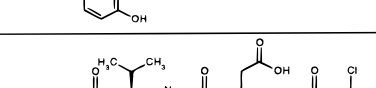
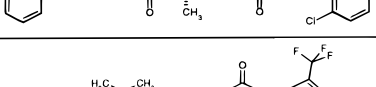
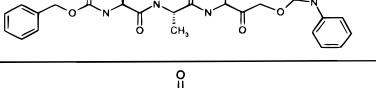
**Materials.** Ac-L-Tyr-L-Val-L-Ala-(D,L)Asp-CHO (compound **4**, Table 1) and Ac-L-Tyr-L-Val-L-Ala-L-Asp-Amc were purchased from Bachem Biosciences (Philadelphia, PA). 7-Amino-4-methyl coumarin (Amc) was purchased from Aldrich Chemical Co. (St. Louis, MO). DTT was purchased from Gibco BRL (Gathersville, MD). Caspase-1 inhibitors were a generous gift from Parke-Davis Pharmaceuticals (Ann Arbor, MI). Compounds **1** and **7** (Table 1) were prepared as described previously (1). Compounds **2** and **3** were prepared by methods described by Mjalli et al. (21, 22). Compounds **5** and **6** were prepared as described by Dolle (14, 23).

**Enzyme Preparation.** Preparation of the autolytically stable caspase-1 variant used in these studies has been described previously (1). Briefly, the variant contains a mutation (D381E) which renders it resistant to autolytic inactivation but has no detectable effect on enzyme activity as compared to the naturally occurring enzyme (24). The

\* Tel: 508-849-2621. Fax: 508-754-7784. E-mail: bradykd@basf.com.

<sup>1</sup> Abbreviations: Amc, 7-amino-4-methyl coumarin; BSA, bovine serum albumin; DTT, dithiothreitol; EDTA, ethylenediaminetetraacetic acid; HEPES, 4-(2-hydroxyethyl)-1-piperazineethanesulfonic acid; rfu, relative fluorescence units.

Table 1: Selected Caspase-1 Inhibitors

Compound	Structure
1	
2	
3	
4	
5	
6	
7	

enzyme variant was expressed in *Escherichia coli*, purified first by immobilized metal chromatography via the N-terminal N-His tag, treated with excess oxidized glutathione to stabilize the reactive thiolate, and then repurified by size-exclusion chromatography. The enzyme is rapidly activated upon exposure to DTT (1).

**Progress Curve Assays.** Serial dilutions of each compound were prepared using an initial 8-fold dilution of a DMSO stock into HGE (100 mM HEPES; 20% glycerol, v/v; and 0.5 mM EDTA), followed by seven serial 2-fold dilutions into HGE + 12.5% DMSO, thus maintaining constant DMSO through the dilution series. Ten microliters of diluted stocks or of vehicle (HGE + 12.5% DMSO) was placed in triplicate onto a 96-well microtiter plate, allowing four compounds to be tested on each plate. The plate was covered to minimize evaporation, and the plate was prewarmed to 30 °C for 20 min. Enzyme was diluted into 10.0 mL of assay buffer (HGE and 5 mM DTT, plus Ac-YVAD-Amc at 15 or 150 μM, as specified; 0.5 nM final enzyme concentration, prewarmed to 30 °C), and this activated reaction mixture was added to the plate at 90 μL/well. Progress of substrate hydrolysis was monitored for 5400 s in a LabSystems (Needham, MA) Fluoroskan Ascent fluorescent plate reader using 385- and 460-nm excitation and emission filters, respectively, and a photomultiplier gain setting of 10. Triplicate curves were averaged and fit by nonlinear regression to eq 1 describing reversible slow-binding inhibition (25) or to eq 2 describing irreversible inactivation:

$$F(t) = F_0 + V_{ss}t + \frac{(V_i - V_{ss})(1 - e^{-k_{obs}t})}{k_{obs}} \quad (1)$$

$$F(t) = F_0 + \frac{V_i(1 - e^{-k_{obs}t})}{k_{obs}} \quad (2)$$

Parameter  $F_0$  was routinely fixed to zero, since fluorescence values were always adjusted to an origin of 0.

Second-order plots ( $k_{obs}$  vs [I]) which demonstrated saturation were analyzed using eq 3 (26):

$$k_{obs} = \frac{k_5[I]}{k_{i,app} + [I]} \quad \text{where} \quad K_i = K_{i,app}/(1 + [S]/K_M) \quad (3)$$

**$k_{off}$  Measurements.** One microliter of compound stock (500 μM in DMSO) and 89 μL of reaction buffer (HGE, 5 mM DTT, and 0.1% BSA, w/v) were combined and warmed to 30 °C, and then 10 μL of NHis(D381E) caspase-1 (1.1 μM in HGE) was added. Reaction mixtures were incubated at 30 °C for 120, 1200, or 2400 s and then applied to Biospin-6 columns (Bio-Rad) which had been preequilibrated with HGE buffer and chilled to 4 °C. The loaded columns were spun for 90 s at moderate speed in a chilled tabletop clinical centrifuge, and eluates were placed on ice. Within 60 s, 10 μL of eluates was added to 390 μL of reactivation assay buffer (HGE, 5 mM DTT, 500 μM Ac-YVAD-Amc, and 0.1% BSA, w/v), and reactivation assays were observed for 1800 s in an Aminco Bowman (Newington, NH) AB2 fluorimeter using 385-nm excitation and 460-nm emission. Duplicate curves were averaged and fit by nonlinear regression to eq 1, and final velocities were expressed as a percentage of the activity recovered after treatment with the fully reversible inhibitor 3. Plots of recovered activity vs reaction time were then modeled as a first-order inactivation of the saturated E–I complex:

$$A(t) = A_0 e^{-kt} \quad (4)$$

**Simulations.** Reaction Scheme 1 was simulated in the context of enzymatic hydrolysis of substrate (Scheme 2). Estimation of kinetic parameters for hydrolysis of AcTyr-ValAlaAsp-Amc was based on (a) the known  $K_M$  of 15 μM and  $k_{cat}$  of approximately 0.7 s<sup>-1</sup> (27, 28) and (b) observations that the truncated substrate analogue AcTyrValAla-NH-(CH<sub>2</sub>)<sub>2</sub>COOH inhibits caspase-1-catalyzed hydrolysis of AcTyrValAlaAsp-Amc with a  $K_i$  of approximately 200 μM (unpublished observations). The ratio  $k_{-1}/k_1$  of 50 μM seemed reasonable since the aminomethylcoumarin group probably enhances binding in the Michaelis complex relative to the truncated peptide (21). The absolute values of  $k_1$  and  $k_{-1}$  are unknown, but the simulation was found not to be significantly affected by the absolute values of these rates for  $k_1 > 10^4$ , and use of these values (which are probably lower than the actual values) permitted use of a larger delta-time during the simulations. The hydration equilibrium is known to occur on the NMR time scale (see Table 3), though neither the absolute rates nor the equilibrium constant is presently known. The rates chosen (Table 4) are probably somewhat slower than the actual rates, but using lower rates stabilized the simulation, and the outcome was found to be

Scheme 2

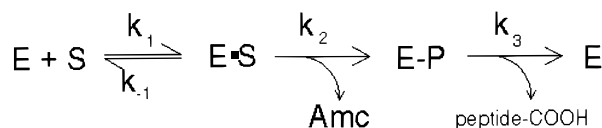


Table 2: Progress Curve Analysis of Selected Caspase-1 Inhibitors

compd	[S] ( $\mu\text{M}$ )	$K_i$ (nM) <sup>a</sup>	$k_5$ ( $\text{s}^{-1} \times 10^3$ ) <sup>a</sup>	$k_{\text{on}}$ ( $\text{M}^{-1} \text{s}^{-1}$ ) <sup>b</sup>
<b>1</b>	15	17 $\pm$ 8	2.9 $\pm$ 0.3	
<b>1</b>	150	13 $\pm$ 2	2.5 $\pm$ 0.2	
<b>2</b>	15	1.9 $\pm$ 0.6	0.41 $\pm$ 0.03	
<b>2</b>	150	2.1 $\pm$ 1.3	0.27 $\pm$ 0.06	
<b>5</b>	150			685 000 $\pm$ 13 000
<b>6</b>	150			582 000 $\pm$ 17 000

<sup>a</sup>  $K_{i,k}$  and  $k_5$  were obtained by fitting the data of Figure 2 (top and middle) to eq 3. Errors represent standard error of the nonlinear regression. <sup>b</sup> Slopes were obtained from Figure 2 (bottom) by linear regression, and errors represent the standard deviation of the regression slope.

Table 3: Proton NMR Chemical Shifts and Peak Widths of **2** and **7** in DMSO- $d_6$  or DMSO- $d_6$ /D<sub>2</sub>O

compd	proton	DMSO- $d_6$		D <sub>2</sub> O	
		shift	width	shift	width
<b>7</b>	–COOH	12.52	sharp	absent	
<b>7</b>	–CH <sub>2</sub> –COOH	2.50–2.83 <sup>a</sup>	sharp	2.6–2.9	broad
<b>2</b>	–COOH	11.9–12.6	broad	absent	
<b>2</b>	–CH <sub>2</sub> –COOH	2.6–2.7 <sup>b</sup>	broad	2.6–2.7	broad

<sup>a</sup> Quartet of doublets. <sup>b</sup> Only half of the quartet is visible, being partly obscured by the ethylene protons.

independent of the absolute rates provided that  $k_{-h} \gg [\text{E}]k_{-4}$ . The  $k_h/k_{-h}$  ratios of 10- or 20-fold excess hydrate are only guesses which serve to illustrate the effects of the hydration equilibrium on the inhibition kinetics.

Simulations were run using Tutsim (Tutsim Products, Palo Alto, CA). Time increments of 1 ms provided stable simulations, and outcomes were not affected by further reductions in the time increment. In the progress curve experiments, substrate hydrolysis was initiated prior to addition of inhibitor. Progress curve simulations were therefore preinitialized by allowing the substrate hydrolysis simulation to reach a steady state (e.g., 8 s of simulation in the absence of inhibitor). This became the starting point for simulations which included inhibitor. For simulations of the recovery curves, substrate concentrations were set to 0, the total inhibitor concentration was set to 5  $\mu\text{M}$ , and the simulation was run for 120, 1200, or 2400 s. These simulations became the starting point for the recovery curve after adjusting the free inhibitor concentrations to 0 and the substrate concentration to 500  $\mu\text{M}$ . Simulated curves were analyzed exactly as described for the analogous experimental data.

## RESULTS

**Kinetics of Inactivation of Caspase-1 by 1.** As demonstrated previously (1), irreversible reaction of **1** (Table 1) with caspase-1 can be monitored by observing fluorimetrically the release of 7-hydroxycoumarin. The rate of 7-hydroxycoumarin release is independent of enzyme concentration, and in accord with Scheme 1 under conditions where the thiohemiketal E–I is saturated, the progress of 7-hy-

Table 4: Simulation of Bimodal Inhibition (Schemes 1 and 2): Input Kinetic Constants,<sup>a</sup> Analysis of Simulated Progress Curve and Reactivation Experiments, and Comparison to Experimental Observations

compd	$k_4$ ( $\text{M}^{-1} \text{s}^{-1}$ )	$k_{-4}$ ( $\text{s}^{-1}$ )	$K_i$ (nM) <sup>c</sup>	$k_5$ ( $\text{s}^{-1} \times 10^3$ )
Simulation Input <sup>b</sup>				
<b>1</b>	2 230 000	0.0026	11.7	0.0010
<b>2</b>	20 000 000	0.0028	2.8	0.00040
Simulation Output <sup>d</sup>				
<b>1</b>	200 000 <sup>e</sup>	0.0035 <sup>f</sup>	17 <sup>g</sup>	1.3 <sup>g</sup> 1.0 <sup>h</sup>
<b>2</b>	1 720 000 <sup>e</sup>	0.0031 <sup>f</sup>	1.8 <sup>g</sup>	0.44 <sup>g</sup> 0.40 <sup>h</sup>
Experimental Observations <sup>i</sup>				
<b>1</b>	160 000 <sup>e</sup>	0.0035 <sup>f</sup>	17 $\pm$ 5 <sup>g</sup>	0.9 $\pm$ 0.03 <sup>j</sup> 2.9 $\pm$ 0.3 <sup>g</sup> 1.0 <sup>h</sup>
<b>2</b>	1 600 000 <sup>e</sup>	0.0031 <sup>f</sup>	1.9 $\pm$ 0.6 <sup>g</sup>	0.41 $\pm$ 0.03 <sup>g</sup> 0.43 <sup>h</sup>

<sup>a</sup> Michaelis–Menton constants for Scheme 2 were  $k_1 = 500\,000 \text{ M}^{-1} \text{s}^{-1}$ ,  $k_{-1} = 25 \text{ s}^{-1}$ ,  $k_2 = 2.33 \text{ s}^{-1}$ , and  $k_3 = 1.0 \text{ s}^{-1}$ . Hydration/cyclization rate constants were  $k_h = 100$  (**1**) or  $200 \text{ s}^{-1}$  (**2**) and  $k_{-h} = 10 \text{ s}^{-1}$  (both compounds). As discussed in the text, the  $k_h$  and  $k_{-h}$  values used for the simulations are probably slower than the actual values, and  $k_h/k_{-h}$  ratios are only guesses which illustrate their effects on the inhibition kinetics. <sup>b</sup> Constants were selected by trial and error to generate simulations which closely match experimental observations in both the progress curve and the reactivation assays. <sup>c</sup>  $K_i$  is defined as the quantity which would be measurable assuming no knowledge of the ketone hydration equilibrium, i.e.,  $K_i = k_h k_{-4} / k_{-h} k_4$ . <sup>d</sup> Simulated data was analyzed in the same manner as the experimental data shown in Figures 1–3. <sup>e</sup>  $k_4$  was calculated as  $k_4 = k_{-4} / K_i$ . <sup>f</sup> Derived from application of eq 1 to the reactivation curves. <sup>g</sup> Progress curves were analyzed using eq 2, and  $K_i$  is the inhibitor concentration at which the inactivation rate is half-maximal (eq 3).  $k_5$  is the maximal inactivation rate found from the second-order plots. <sup>h</sup>  $k_5$  was evaluated from the time-dependent extent of simulated reactivation following incubations with inhibitors, as described for the data of Figure 3. <sup>i</sup> Summarized from Table 2 and Figures 1–3. <sup>j</sup> Rate of 7-hydroxycoumarin release upon reaction of caspase-1 with compound **1** (1).

droxycoumarin release is accurately modeled as a single first-order process (eq 2) with a mean rate of  $(9.0 \pm 0.3) \times 10^{-4} \text{ s}^{-1}$ .

**Kinetics of Inhibition of Caspase-1 by 1.** The kinetics of inhibition of caspase-1 by **1** are complex (Figure 1, top). Notably, early in the assay, when only small amounts of 7-hydroxycoumarin have been released, potent inhibition of substrate hydrolysis is already observed. The fit of the irreversible model (eq 2) to the progress curves appears quite good, though examination of the residuals (Figure 1A, inset) demonstrates that the model consistently predicts greater inhibition at early times than is actually observed. The acyloxymethyl ketone **2** generates a similar pattern of inhibition (Figure 1, middle), i.e., rapid inhibition followed by slow downward curvature in the assays, and a residual pattern which indicates that eq 2 inadequately describes the kinetics at early time points. In contrast, the reversible, slow-binding inhibitor **4** assayed under identical conditions shows a nearly featureless residual (Figure 1, bottom). The flatness of the residuals observed for compound **4** is not due the greater adaptability of the reversible model (eq 1), since the progress curves of the both compounds **1** and **2** show distinctive residual patterns when fitted against either model (data not shown).

Caspase-1 is not an especially efficient enzyme (27, 28), so that the minimal practical enzyme concentration for these

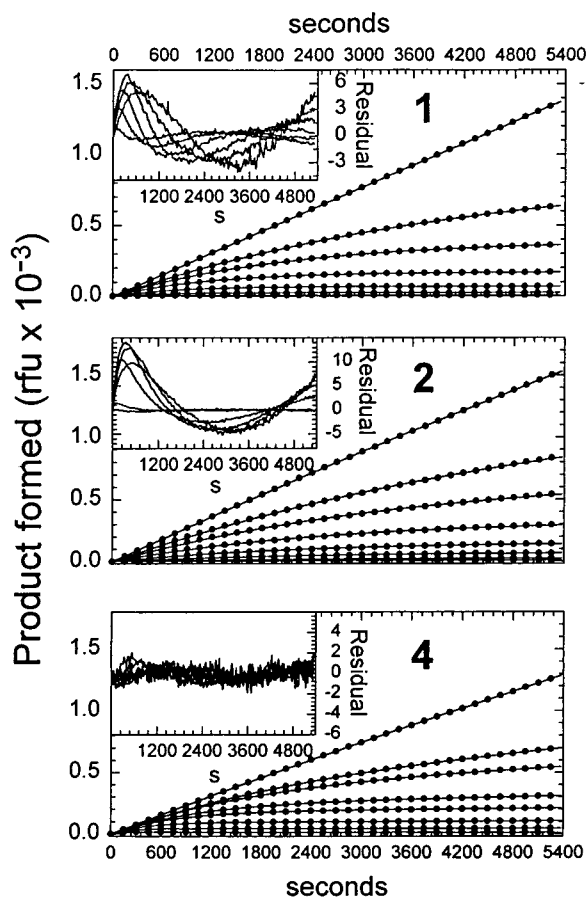


FIGURE 1: Kinetics of inhibition of caspase-1 by **1**, **2**, and **4**. These series of progress curves were obtained using a substrate concentration of 15  $\mu\text{M}$  and inhibitor concentrations of 0, 3.9, 7.8, 15.6, 31.3, 62.5, 125, and 250 nM. The solid circles represent data points (only every fifth point is shown for clarity), and solid lines represent best fits to eq 2 (compounds **1** and **2**) or eq 1 (compound **4**). Insets: Residuals from the curve-fitting analyses show that at early times, enzyme is consistently more inhibited by compounds **1** and **2** than is predicted by the model function, while residuals for the reversible, slow-binding inhibitor **4** are featureless.

assays is just below 1 nM, and reaction conditions at the lowest inhibitor concentration (3.9 nM) cannot be considered “pseudo-first-order”. To alleviate this possible problem, these assays were repeated using 150  $\mu\text{M}$  substrate, thereby reducing by 10-fold the amount of free enzyme present at any time during the assay. While the overall inhibitory reaction rates were markedly reduced, a qualitatively similar departure from the model (eq 2) was observed in the residuals (data not shown). Furthermore, the departure from the model observed for both compounds **1** and **2** is clearly observed at inhibitor concentrations as high as 62.5 nM (Figure 1), a concentration which easily meets the criterion for pseudo-first order conditions.

Noting that the aldehyde inhibitor **4** is “slow-binding”, we expected that the complex kinetics of **1** and **2** might arise from a superimposition of slow, reversible inhibition and slower inactivation, i.e.,  $k_4[\text{I}] \sim k_5$  (Scheme 1). We therefore sought to measure the rate and equilibrium constants involved in each step of Scheme 1.

**Second-Order Plots of Compounds 1, 2, 5, and 6.** Second-order plots ( $k_{\text{obs}}$  vs  $[\text{I}]$ ) for the bimodal inhibitors **1** and **2** and, for comparison, the inactivators **5** and **6** are shown in Figure 2. Kinetic constants derived from these plots are

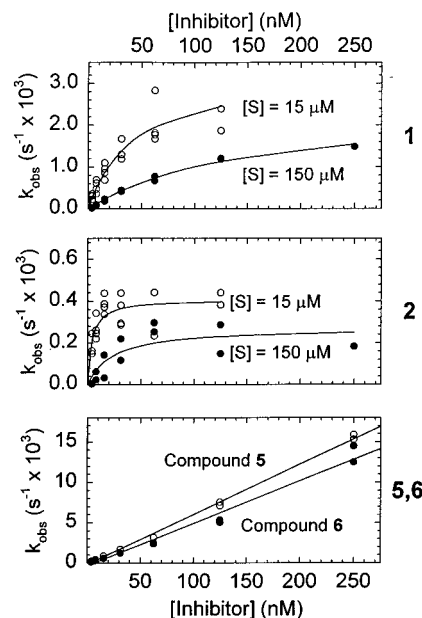


FIGURE 2: Second-order plots of bimodal (**1**, **2**) and irreversible (**5**, **6**) inhibitors. Top and middle:  $k_{\text{obs}}$  derived from progress curve assays (Figure 1 and data not shown) at low ( $[\text{Ac-YVAD-Amc}] = 15 \mu\text{M}$ , open circles) and high ( $[\text{Ac-YVAD-Amc}] = 150 \mu\text{M}$ , closed circles) substrate concentrations are plotted as a function of inhibitor concentration. Data shown were accumulated from 2–4 independent experiments for each inhibitor, and curves were rejected from the analysis when the signal was too weak to yield meaningful data (e.g., at the highest inhibitor concentrations). Data were fit to eq 3, and best parameters are described in the text and Table 2. Bottom: Progress curve assays were run in the presence of 150  $\mu\text{M}$  Ac-YVAD-Amc.  $k_{\text{on}}$  values for **5** (○) and **6** (●) were determined from the slopes as evaluated by linear regression and are summarized in Table 2.

summarized in Table 2. Both compounds **1** and **2** clearly demonstrate saturation kinetics. Compound **1** inhibited caspase-1 at a maximal rate of  $k_5 = 2.9 \times 10^{-3} \text{ s}^{-1}$  (or  $2.5 \times 10^{-3} \text{ s}^{-1}$  when measured at 150  $\mu\text{M}$  substrate), and inactivation was half-saturated at  $K_i = 17 \text{ nM}$  (or 13 nM when measured at 150  $\mu\text{M}$  substrate; all  $K_i$  values are corrected by  $1/(1 + [\text{S}]/K_M)$  since these inhibitors are known to be competitive with substrate). In contrast, **2** was a slower inactivator ( $k_5 = 4.1 \times 10^{-4}$  or  $2.7 \times 10^{-4} \text{ s}^{-1}$  at 15 or 150  $\mu\text{M}$  substrate, respectively) but saturated the enzyme more potently ( $K_i = 1.9$  or 2.1 nM at 15 or 150  $\mu\text{M}$  substrate, respectively).

The inactivators **5** and **6** were assayed using 150  $\mu\text{M}$  substrate, since this condition retards the inactivation reaction and improves accuracy in the measurements. The second-order plots of both compounds failed to saturate at inhibitor concentrations as high as 250 nM, as would be expected when  $k_5 \gg k_4[\text{I}]$ . We observe inactivation rates of 685 000 and 582 000  $\text{M}^{-1} \text{ s}^{-1}$  for **5** and **6**, respectively, which compare reasonably to  $k_{\text{obs}}/[\text{I}]$  values reported previously (14, 23), though these measurements were obtained under significantly different conditions and protocols than ours.

**Reactivation of Caspase-1 after Inhibition by Selected Inhibitors.** To demonstrate directly that the early phase of inhibition by the ketones **1** and **2** is reversible, and to measure directly the rate constants  $k_{-4}$  and  $k_5$  (Scheme 1), enzyme was treated with inhibitor (500  $\mu\text{M}$ ) for 120, 1200, or 2400 s; chilled and passed by centrifugation through a miniature size-exclusion column to remove free inhibitor; and then

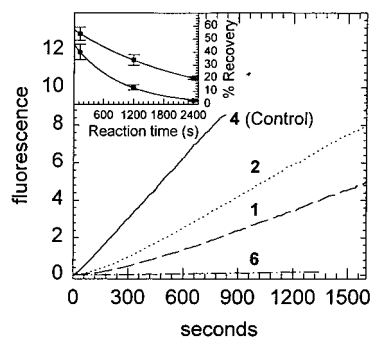


FIGURE 3: Recovery from inhibition after treatment with bimodal inhibitors. Caspase-1 treated with inhibitor ( $5 \mu\text{M}$ ) in HGDE buffer for 120 s was chilled and separated from excess inhibitor by rapid size-exclusion chromatography and then assayed in HGDE containing  $500 \mu\text{M}$  Ac-YVAD-Amc. Reactivation curves following the 1200- and 2400-s reactions are not shown. Curves were analyzed using eq 1, yielding reactivation rates of  $(3.1 \pm 0.4) \times 10^{-3}$  and  $(3.5 \pm 1.5) \times 10^{-3} \text{ s}^{-1}$  for **1** and **2**, respectively. Inset: Maximal reactivation expressed as a percentage of the control reaction is plotted as a function of reaction time. Error bars represent the standard deviation of triplicate (120 s only) or duplicate measurements. The solid curves are the best fits to eq 4, giving the parameters  $k = 1.0 \times 10^{-3} \text{ s}^{-1}$  and  $A_0 = 45\%$  for **1** and  $k = 0.43 \times 10^{-3} \text{ s}^{-1}$  and  $A_0 = 57\%$  for **2**.

assayed in the presence of excess substrate to observe recovery of activity. The recovery curves of compounds **1**, **2**, **3**, and **6** after 120-s reactions are shown in Figure 3, and the inset shows the percentage of activity recovered relative to the fully reversible control inhibitor **3** (**21**) after each reaction time. Transient upward curvature was observed in the recovery from inhibition by **3**, but the rate was too fast to be reliably measured by this technique.

Caspase-1 could be partially reactivated after treatment with either of the bimodal inhibitors **1** or **2** (Figure 2), and reactivation rates were approximately  $3\text{--}3.5 \times 10^{-3} \text{ s}^{-1}$  for both compounds, a value interpreted as  $k_{-4}$  in Scheme 1. After longer reaction intervals, enzyme activity was still recoverable, though at lower levels than after the short reaction. This was entirely expected for **1**, since the titration data clearly demonstrate that the 7-hydroxycoumarin group leaves with a rate constant of  $(9.0 \pm 0.3) \times 10^{-4} \text{ s}^{-1}$  ( $t_{1/2} = 770 \text{ s}$ ). A compound very closely related to compound **2** has been described as reversible (**22**), but the current experiment, as well as the second-order plot (Figure 2), indicates clearly that compound **2** is a bimodal inhibitor, capable of irreversible inactivation of the enzyme, although at a rather slower rate. Analysis of the percentage recovery vs time using a model for first-order inactivation of the enzyme–inhibitor complex (eq 4) provides estimates of  $k_5$  which are quite close to values from the titration experiments (*I*) and the second-order plots of progress curve assays (Figure 2). Notably, the total recoverable activity extrapolated to  $t = 0$  ( $A_0$ ) is only about 50%. This results, in part, from the bimodal nature of these inhibitors, since the inactivation of the *E*–*I* complex continues throughout the assay. Since the reactivation rate ( $k_{-4}$ ) is only slightly faster than the inactivation rate ( $k_5$ ), this causes an apparent decrease in the total recoverable activity, especially after short reaction times. This problem is more severe for compound **1** ( $A_0 = 45\%$ ) than for compound **2** ( $A_0 = 57\%$ ) since the inactivation rate of **1** ( $k_5 = 0.0010$ ) is only slightly smaller than the reactivation rate ( $k_4 = 0.0031 \text{ s}^{-1}$ ). Equation

1, which is more properly applied to reactivation curves of fully reversible complexes, can only approximate the reactivation after treatment with these bimodal inhibitors. Simulations confirm that the results of these analyses are at least reasonable but that the apparent  $k_{-4}$  derived using eq 1 slightly overestimates the true value, especially for compound **1** (see below).

Activity was never recovered after treatment with the potent inactivator **5** (data not shown), but low levels of activity were recovered after brief treatment with the (1-phenyl-3-(trifluoromethyl)pyrazol-5-yl)oxy ketone **6** (**14**), suggesting that this class of inhibitor may act via Scheme 1 with very fast progression to the irreversible adduct (e.g.,  $k_5 \approx 0.036 \text{ s}^{-1}$ , based on the single observable time point in Figure 3).

**The Role of Ketone Hydration and Intramolecular Cyclization Equilibria.** Ketone analogues of aspartic acid are capable of hydrating to a hemiketal or of cyclizing to form a stable 5-membered ring as depicted in the left section of Scheme 1. The degree to which the cyclic adduct and hydrate form is a function of the ketone carbonyl's electrophilic character and of the nature of the solvent in which the inhibitor is dissolved. In our assay system, we have intentionally allowed the inhibitors (normally stored in DMSO stock solutions) to incubate in assay buffer so that equilibrium is attained prior to addition of enzyme and substrate. In  $^1\text{H}$  and  $^{13}\text{C}$  NMR spectra of **7** dissolved in DMSO- $d_6$ , resonances of both the COOH proton and the methylene protons attached to the aspartic acid  $\beta$ -carbon are relatively sharp, and the ketone carbonyl is readily observed in the  $^{13}\text{C}$  spectrum (Table 3 and data not shown). Addition of 0.2 vol of  $\text{D}_2\text{O}$  causes complete disappearance of the carboxylate proton and  $^{13}\text{C}$  ketone resonances, as well as broadening of the  $\beta$ -methylene protons. In contrast, even in pure DMSO, compound **2** shows broadened  $\beta$ -methylene proton resonances, a greatly broadened COOH resonance, and an absent  $^{13}\text{C}$  ketone resonance (data not shown). Addition of  $\text{D}_2\text{O}$  to the DMSO solution of **2** had no further effect. Thus, in aqueous assay buffer, both ketones **1** and (especially) **2** are expected to be in equilibrium which favors cyclized and/or hydrated forms, and this equilibrium is established at a time scale on the order of milliseconds, as evidenced by the broadening observed over the NMR time scale.

To test whether equilibria established during mixing might affect the kinetic profile, we ran assays using a slightly modified protocol such that the inhibitor remained in DMSO solvent until addition of the activated enzyme. Since DMSO favors the free ketone form of the inhibitor, we expected that the initial lag in inhibition might be reduced or abolished in these assays. However, no significant differences were observed between assays using DMSO solvent and those using a preequilibration in the aqueous assay buffer (data not shown). Thus, these reversible equilibria involving the ketone functionality are unlikely to play a significant role in the observed kinetic profiles other than causing a reduction in the observable  $k_4$  (Scheme 1) by reducing the amount of reactive ketone present.

**Simulations of Scheme 1.** The models generally used to describe the progress curve assays (eqs 1 and 2) do not entirely describe the kinetics of inhibition by potent, bimodal inhibitors, as these inhibitors display combined properties

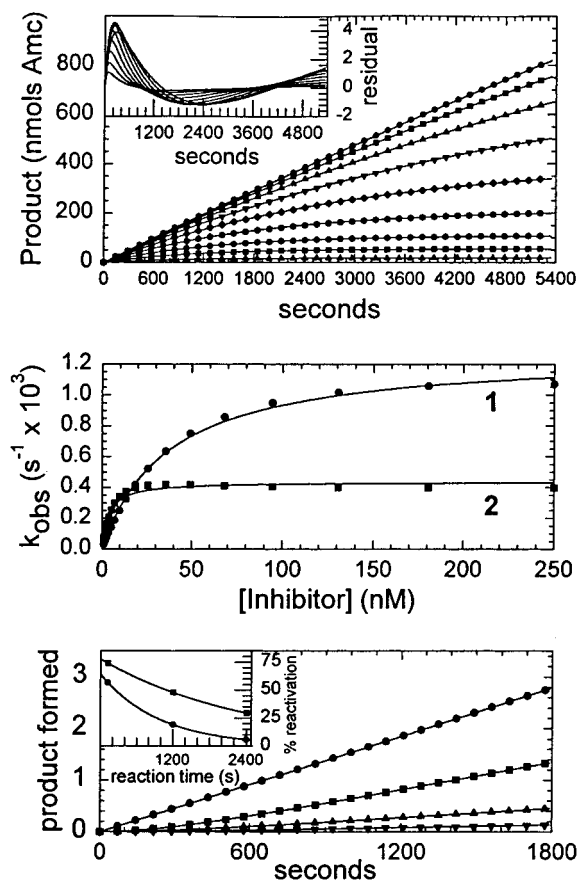


FIGURE 4: Simulation of bimodal inhibition. Parameters used for simulations are summarized in Table 4. Top: Simulated progress curves for compound 1. Symbols represent simulated data at evenly distributed inhibitor concentrations between 1 and 250 nM, and solid curves are the best fits to eq 2. Top, inset: Residuals from the best fit to eq 2 demonstrating similarity to experimental residuals (Figure 1). Middle: Second-order plots of simulated progress curves for compounds 1 and 2. The best fit to eq 3 provides the values in Table 4. Bottom: Simulated reactivation experiments for compound 1 after 120- and 1200-s reactions. Bottom, inset: Plot of percent reactivation vs reaction time for compounds 1 and 2. Smooth curves represent best fits to eq 4, providing the reactivation rates ( $k_{-4}$ ) in Table 4.

of slow-binding reversible and slow-inactivating inhibitors. Similarly, eqs 1 and 4 do not accurately model the recovery from inhibition by 1 or 2 (Figure 3) since enzyme inactivation continues at a rate proportional to the remaining E-I complex throughout the reactivation time course. To gauge the validity of the kinetic constants derived from application of these models (Tables 2 and 3), we have used the simulation tool Tutsim to generate simulated data which closely resemble our experimental data. We have then analyzed these data in the same manner as the experimental data and compared the outcome of this analysis with the parameters which were applied to the simulation. The results of this exercise are shown in Figure 4 and Table 4. Reasonably good agreement is observed between the kinetic constants entered into the simulation and the constants derived analytically from the simulated progress curves and reactivation curves. However, systematic errors are identified in both the progress curve and the reactivation experiments.

In the simulated second-order plots (Figure 4, top and middle),  $k_{\text{obs}}$  slightly overshoots  $k_5$ . This overshoot occurs because at low to intermediate inhibitor concentrations the

“reversible slow-binding” phenomenon (observable in Figures 1 and 4 as a positive deviation from the model) influences the nonlinear regression analysis. If it were possible to separate completely this portion of the curves from the subsequent inactivation process,  $k_{\text{obs}}$  values would reflect the reversible process (i.e.,  $k_{\text{obs}} = k_4[\text{I}]$  for a fully reversible inhibitor). The overshoot occurs in the experimental range where  $k_4[\text{I}] \gg k_5$  and  $k_4[\text{I}]$  is sufficiently small to be observable given the time scale of the experiment and the sensitivity of the instrumentation. Overshoot is not particularly noticeable in Figure 2, which is a composite of multiple experiments, but in individual series of progress curves, overshoot is frequently observed for these and related compounds (unpublished observations).

The measured  $K_i$  is affected by this overshoot. The second-order plot for compound 1 is affected by the overshoot at concentrations as high as 130 nM, so that both  $K_i$  and  $k_5$  are overestimated by as much as 50%. In contrast, the overshoot for compound 2 completes early in the plot, so that a large portion of the data occurs in a range where  $k_{\text{obs}}$  approaches  $k_5$  asymptotically and generates a more accurate estimate of both  $K_i$  and  $k_5$ . Fortunately, the reactivation time course (Figure 3) provides an alternative experimental technique which does provide an accurate estimate of  $k_5$  which is applicable to most compounds of this mechanistic class.

Finally,  $k_{-4}$  derived from the reactivation curves overestimates the actual value by 35% (compound 1) or 10% (compound 2). The severity of the overestimation thus appears to be related to the closeness of the true  $k_{-4}$  to the inactivation rate,  $k_5$ , so that eq 1, which accurately describes slow recovery from fully reversible inhibition, no longer approximates recovery from bimodal inhibition.

## DISCUSSION

Preliminary progress curve analyses of the action of these bimodal inhibitors using a single-cuvette fluorimeter often provided data which seemed to indicate overshoot in the second-order plots (unpublished observations), but the signal/noise ratio of the fluorescence vs time traces was usually too poor to discern the cause of this overshoot. Implementation of progress curve assays in a microtiter plate format has generated high-quality fluorescence data from multiple wells, and signal averaging has reduced the noise level sufficiently to observe the complex kinetic pattern by residual analysis (Figure 1). Use of a stabilized preparation of caspase-1 (I) was also essential, since enzyme stability imposes a limit on the lowest detectable inactivation rate. For example, application of eq 2 to the vehicle control progress curves yields a  $k_{\text{obs}}$  on the order of  $2 \times 10^{-5} \text{ s}^{-1}$ , which likely reflects the rate of inactivation of enzyme by nonspecific processes. The saturation kinetic profile of relatively slow compounds such as 2 is thereby readily observable (Figure 2), and maximal inactivation rates ( $k_5$ ) as low as  $2 \times 10^{-4} \text{ s}^{-1}$  can be reproducibly measured (unpublished observations).

This study has detailed the actions of two caspase-1 inhibitors and suggests that their kinetic profiles result from the superimposition of reversible slow-binding inhibition followed by slower inactivation. Simulations have then demonstrated that Scheme 1 is able to generate kinetic

profiles which closely match the experimental observations. Scheme 1 assumes that attack by the sulfur upon the nearby methylene carbon occurs directly from the thiohemiketal complex, forming a transient cyclic sulfonium intermediate (12). An alternative mechanism wherein a noncovalent enzyme/inhibitor complex partitions between reversible thiohemiketal formation and irreversible thioether formation cannot yet be discounted. However, several attempts to simulate this mechanism have thus far failed to mimic the experimental observations (unpublished observations). It is also possible that another catalytic residue, such as His 237, might participate in the inactivation reaction, as was demonstrated for the inhibition of the serine protease chymotrypsin by an  $\alpha$ -chloroketone inhibitor (29). However, crystallographic observation of caspase-1 after treatment with bimodal inhibitors such as **1** clearly shows the enzyme covalently linked via Cys 285 to the  $\alpha$ -methylene carbon (30; N. P. Walker, personal communication).

Working with a series of acyloxymethyl ketone inhibitors of cathepsin B, Krantz et al. were able to demonstrate a strong correlation between the leaving group  $pK_a$  and the inactivation rate,  $\log(k_5/K_i)$  (12). In contrast, Thornberry et al. demonstrated that for a series of tripeptide benzoyloxymethyl ketone inhibitors of caspase-1, overall inactivation rate (i.e.,  $k_5/K_i$ ) was not correlated with leaving group  $pK_a$  and that binding of these inhibitors to the enzyme was the rate-limiting step in the inactivation (31). While this latter study failed to account for counteracting effects of the leaving group  $pK_a$  on the degree of ketone hydration/cyclization which might diminish or mask a correlation with the inactivation rate, this study's observation of slow-binding kinetics for the reversible phase of inhibition by compounds **1** and **2** does support their conclusion that an apparently slow binding step precedes the inactivation of caspase-1 by this class of inhibitors. However, it is not yet clear whether this binding step is intrinsically slow, or whether it only appears slow due to a high degree of hydration/cyclization of the inhibitory ketone species. It furthermore remains to be demonstrated whether "inactivators", such as compounds **5** and **6**, might display saturation kinetics if techniques appropriate for observing time constants  $> 0.030 \text{ s}^{-1}$  were applied.

The leaving groups of inhibitors **1** and **2** have  $pK_a$  values of approximately 8 (32) and 4.5, respectively. Nevertheless, compound **2** ( $k_5 = 0.4 \times 10^{-4} \text{ s}^{-1}$ ) inactivates caspase-1 over 2-fold more slowly than **1** ( $k_5 = 9 \times 10^{-4} \text{ s}^{-1}$ ). All other factors being equal, the  $\beta$ -oxygen of **2** should be more susceptible to  $SN_2$  displacement than that of **1**. A likely explanation for this anomaly is that geometric constraints resulting from specific binding interactions of the leaving group dominate the inactivation kinetics ( $k_5$ ) of these inhibitors. Indeed, inspection of the crystallographic structures of caspase-1 complexed with reversible ketone inhibitors bearing a variety of linkages to the  $\alpha$ -methylene carbon (e.g., aliphatic, alkyl- and arylthioether, aryl ether, and acyloxy) reveals a common geometry and stereochemistry for the thiohemiketal center with multiple geometries for the attachment to the  $\alpha$ -methylene carbon (N. P. Walker, personal communication). The precise alignment between the Cys 285 sulfur, the  $\alpha$ -methylene carbon, and the charge-bearing leaving group atom is expected to be a critical determinant in the net rate of the displacement reaction.

## CONCLUSIONS

Aryloxymethyl and acyloxymethyl ketones are promising for their potential pharmaceutical applications as inhibitors of caspase-1 and other cysteine proteases with key roles in pathogenic processes. The dual electrophilic centers of these inhibitors provide the potential to act in a combination of reversible and/or irreversible modes and generate complex kinetic profiles which are not fully described by the analytical models. Careful observation of the quality of fit to these models combined with direct measurements of time-dependent reversal of inhibition has provided an accurate assessment of the separate contributions of the reversible and irreversible inhibitory modes to the action of these inhibitors. A more complete understanding of the specific binding interactions achieved by potential leaving groups can hopefully be applied to the development of more specific inhibitors and safer pharmaceutical compositions.

## ACKNOWLEDGMENT

Thanks to Chris Grinnell and David Banach for enzyme preparation; Luke Jiang for the NMR studies; and Catherine Kostlan, Robert Talanian, and Nigel Walker for many insightful discussions of the practical and theoretical aspects of this work. Special thanks to John Gilmore for synthesis of the caspase-1 inhibitors.

## REFERENCES

- Dang, L. C., Talanian, R. V., Banach, D., Hackett, M. C., Gilmore, J. L., Hays, S. J., Mankovich, J. A., and Brady, K. D. (1996) *Biochemistry* 35 (47), 14910–14916.
- Rasnick, D. (1996) *Perspect. Drug Discovery Des.* 6, 47–63.
- Otto, H.-H., and Schirmeister, T. (1997) *Chem. Rev.* 97 (1), 133–171.
- Okamura, H., Tsutsui, H., Komatsu, T., Yutsudo, M., Hakura, A., Tanimoto, T., Kakuiji, T., Okura, T., Nukada, Y., Hattori, K., Akita, K., Namba, M., Tanabe, F., Konishi, K., Fukuda, S., and Kurimoto, M. (1995) *Nature* 378, 88–90.
- Gu, Y., Kuida, K., Tsutsui, H., Ku, G., Hsiao, K., Fleming, M. A., Hayashi, N., Higashino, K., Okamura, H., Nakanishi, K., Kurimoto, M., Tanimoto, T., Flavell, R. A., Sato, V., Harding, M. W., Livingston, D. J., and Su, M. S.-S. (1997) *Science* 275, 206–209.
- Ghayur, T., Banerjee, S., Hugunin, M., Butler, D., Herzog, L., Carter, A., Quintal, L., Sekut, L., Talanian, R., Paskind, M., Wong, W., Kamen, R., Tracey, D., and Hamish, A. (1997) *Nature* 386 (6625), 619–623.
- Li, P., Allen, H., Banerjee, S., Franklin, S., Herzog, L., Johnston, C., McDowell, J., Paskind, M., Rodman, L., Salfeld, J., Towne, E., Tracey, D., Wardwell, S., Wei, F.-Y., Wong, W., Kamen, R., and Seshadri, T. (1995) *Cell* 80, 401–411.
- Kuida, K., Lippke, J. A., Ku, G., Harding, M. W., Livingston, D. J., Su, M. S.-S., and Flavell, R. A. (1995) *Science* 267, 2000–2003.
- Stosic-Grujicic, S., Basara, N., Milenkovic, P., and Dinarello, C. A. (1995) *J. Chemother.* 7 (1), 67–70.
- Estrov, Z., and Talpaz, M. (1996) *Drug News & Perspect.* 9 (1), 5–12.
- Smith, R. A., Copp, L. J., Coles, P. J., Pauls, H. W., Robinson, V. J., Spencer, R. W., Heard, S. B., and Krantz, A. (1988) *J. Am. Chem. Soc.* 110, 4429–4431.
- Krantz, A., Copp, L. J., Coles, P. J., Smith, R. A., and Heard, S. B. (1991) *Biochemistry* 30, 4678–4687.
- Pliura, D. H., Bonaventura, B. J., Smith, R. A., Coles, P. J., and Krantz, A. (1992) *Biochem. J.* 288 (3), 759–762.

14. Dolle, R. E., Singh, J., Rinker, J., Hoyer, D., Prasad, C. V. C., Graybill, T. L., Salvino, J. M., Helaszek, C. T., Miller, R. E., and Ator, M. A. (1994) *J. Med. Chem.* 37 (23), 3863–3866.
15. Dolle, R. E., Singh, J., Whipple, D., Osifo, I. K., Speier, G., Graybill, T. L., Gregory, J. S., Harris, A. L., Helaszek, C. T., Miller, R. E., and Ator, M. A. (1995) *J. Med. Chem.* 38, 220–222.
16. Graybill, T. L., Prouty, C. P., Speier, G. J., Hoyer, D., Dolle, R. E., Helaszek, C. T., Ator, M. A., Uhl, J., and Strasters, J. (1997) *Bioorg. Med. Chem. Lett.* 7 (1), 41–46.
17. Dolle, R. E., Prasad, C. V. C., Prouty, C. P., Salvino, J. M., Awad, M. M. A., Schmidt, S. J., Hoyer, D., Ross, T. M., Graybill, T. L., Speier, G. J., Uhl, J., Miller, B. E., Helaszek, C. T., and Ator, M. A. (1997) *J. Med. Chem.* 40 (13), 1941–1946.
18. Semple, G., Ashworth, D. M., Baker, G. R., Batt, A. R., Baxter, A. J., Benzie, D. W. M., Elliot, L. H., Evans, D. M., Franklin, R. J., Hudson, P., Jenkins, P. D., Pitt, G. R., Rooker, D. P., Sheppard, A., Szelke, M., Yamamoto, S., and Isomura, Y. (1997) *Bioorg. Med. Chem. Lett.* 7 (10), 1337–1342.
19. Mjalli, A. M. M., Zhao, J. J., Chapman, K. T., Thornberry, N. A., Peterson, E. P., MacCoss, M., and Hagmann, W. K. (1995) *Bioorg. Med. Chem. Lett.* 5 (13), 1409–1414.
20. Brömme, D., Smith, R. A., Coles, P. J., Kirschke, H., Storer, A. C., and Krantz, A. (1994) *Biol. Chem. Hoppe-Seyler* 374, 343–347.
21. Mjalli, A. M. M., Chapman, K. T., MacCoss, M., and Thornberry, N. A. (1993) *Bioorg. Med. Chem. Lett.* 3 (12), 2689–2692.
22. Mjalli, A. M. M., Chapman, K. T., MacCoss, M., Thornberry, N. A., and Peterson, E. P. (1994) *Bioorg. Med. Chem. Lett.* 4 (16), 1965–1968.
23. Dolle, R. E., Hoyer, D., Prasad, C. V. C., Schmidt, S. J., Helaszek, C. T., Miller, R. E., and Ator, M. A. (1994) *J. Med. Chem.* 37, 563–564.
24. Thornberry, N. A., Bull, H. G., Calaycay, J. R., Chapman, K. T., Howard, A. D., Kostura, M. J., Miller, D. K., Molineaux, S. M., Weidner, J. R., Aunins, J., et al. (1992) *Nature* 356 (6372), 768–774.
25. Cha, S. (1975) *Biochem. Pharmacol.* 24, 2177–2185.
26. Palmer, J. T., Rasnick, D., Klaus, J. L., and Brömme, D. (1995) *J. Med. Chem.* 38 (17), 3193–3196.
27. Giegel, D. A. (1997) *J. Cell. Biochem.* 64 (1), 11–18.
28. Thornberry, N. A. (1994) *Methods Enzymol.* 244 (31), 615–631.
29. Kreutter, K., Steinmetz, A. C., Liang, T. C., Prorok, M., Abeles, R. H., and Ringe, D. (1994) *Biochemistry* 33 (46), 13792–13800.
30. Walker, N. P. C., Talanian, R. V., Brady, K. D., Dang, L. C., Bump, N. J., Ferenz, C. R., Franklin, S., Ghayur, T., Hackett, M. C., Hammill, L. D., Herzog, L., Hugunin, M., Houy, W., Mankovich, J. A., McGuinness, L., Orlewicz, E., Paskind, M., Pratt, C. A., Reis, P., Summani, A., Terranova, M., Welch, J. P., Xiong, L., Möller, A., Tracey, D. E., Kamen, R., and Wong, W. W. (1994) *Cell* 78, 343–352.
31. Thornberry, N. A., Peterson, E. P., Zhao, J. J., Howard, A. D., Griffin, P. R., and Chapman, K. T. (1994) *Biochemistry* 33, 3934–3940.
32. Rosenberg, D. W., Roque, H., and Kappas, A. (1990) *Anal. Biochem.* 191, 354–358.

BI9803325